

Thermoviscous Effects in Steady and Oscillating Flow of Superfluid ^4He : Experiments

S. Backhaus, K. Schwab,* A. Loshak, S. Pereverzev,† N. Bruckner,
J. C. Davis, and R. E. Packard

Physics Department, University of California, Berkeley, California 94720, USA

(Received April 16, 1997; revised July 9, 1997)

The correct interpretation of superfluid flow experiments relies on the knowledge of thermal and viscous effects that can cause deviations from ideal behavior. The previous paper presented a theoretical study of dissipative and reactive (nondissipative) thermoviscous effects in both steady and oscillating flow of an isotropic superfluid through small apertures and channels. Here, a detailed comparison is made between the theory and a wide array of experimental data. First, the calculated resistance to steady superflow is compared with measurements taken in a constant pressure-head flow cell. Second, the resonant frequency and Q of three different Helmholtz oscillators are compared with predictions based on the calculated frequency response. The resonant frequency and Q are extracted numerically from the frequency response, and analytical results are given in experimentally important limits. Finally, the measured and calculated frequency response are compared at a temperature where the Helmholtz oscillator differs significantly from a simple harmonic oscillator. This difference is used to explain how the thermal properties of the oscillator affect its response. The quantitative agreement between the theory and experiment provide an excellent check of the previously derived equations. Also, the limiting expressions shown in this paper provide simple analytical expressions for calculating the effects of the various physical phenomena in a particular experimental situation.

1. INTRODUCTION

Superfluid hydrodynamics has been studied almost since the discovery of the superfluidity of ^4He .² Much of this work has been focused on the

* Present address: Condensed Matter Physics 114-36, California Institute of Technology, Pasadena, California 91125, USA.

† Permanent address: Institute for High Pressure Physics, Russian Academy of Sciences, Russia.

problem of the critical velocity, v_c , the velocity at which the superfluid begins to dissipate large amounts of flow energy. This paper focuses on the region below the critical velocity where, depending on the flow geometry, superflow may be accompanied by several dissipative processes. The geometry which will prove to be dissipative consists of relatively open regions, which allow normal fluid flow, connected by narrow channels that at least partially lock the normal fluid. Superflow through the channel creates a temperature difference between the open regions by changing their specific entropy. The temperature difference relaxes by thermal conduction through the container walls. Although the superflow itself remains dissipationless, the irreversible flow of heat causes dissipation. The temperature difference also creates a chemical potential difference which must be taken into account to correctly interpret a superflow experiment. Also, if the normal fluid is partially free to move, it dissipates energy through viscous losses.

The equations of motion which govern flow in geometries similar to the one mentioned above are derived in Ref. 1. The end results of that calculation, which are repeated here, are the subcritical resistance to steady superflow

$$\mathcal{R} \equiv \frac{\Delta P}{i} = \left[\frac{1}{\rho_S^2 T R_T} + \frac{1}{R_\eta} \right]^{-1} \quad (1)$$

and the frequency response of a Helmholtz oscillator

$$\tilde{x}(\omega) = \frac{\tilde{F}_c}{k} \frac{H(\Omega_c, \Gamma_c, \Phi_c, \Lambda_c, \Sigma_c)}{H(\Omega_h, \Gamma_h, \Phi_h, \Lambda_h, \Sigma_h)}. \quad (2)$$

The expression for H is given by Eq. 29 of Ref. 1. For a definition of all symbols used in this paper, see the Appendix.

In this paper, we will apply these results to several different experimental situations. First, we will investigate steady flow driven by a recently developed constant pressure-head flow cell.⁴ The data from this cell allows a quantitative check of the subcritical resistance given in Eq. 1. Second, we will compare the resonant frequency and Q of three different Helmholtz oscillators^{5,6} with theoretical results obtained from the frequency response given by Eq. 2. The resonant frequency and Q are extracted numerically from the calculated frequency response, and analytical results are given in experimentally important limits. For one of the oscillators, we compare not only the resonant frequency and Q , but also the frequency response. The comparison is made at a temperature where the response has significant differences from the response of a simple harmonic oscillator. This difference is then used to explain some of the properties of this type of oscillator.

Brooks *et al.*³ have performed similar calculations, but made several simplifying assumptions that restrict their results to adiabatic oscillations

with small thermal effects and nearly locked normal fluid. Also, their results are only valid in a frequency range near the Helmholtz resonance. In Ref. 1, we have not made these simplifications. Comparison of the present results with those of Ref. 3 is made in the appropriate limit.

2. STEADY FLOW

Reference 1 describes an experimental situation where steady superflow can dissipate energy when the superfluid velocity, v_s , is less than v_c . Normally, transient measurements of this region are limited because of the short time the transient spends with $v_s < v_c$.⁵ We have developed a constant pressure-head flow cell⁴ that is able to drive flow with $v_s < v_c$ for long periods of time. This allows us to explore the region below v_c with high precision.

As shown in Fig. 1, the cell consists of two superfluid filled volumes separated by a common wall. Mounted in the wall are two flexible, $8\ \mu\text{m}$ Kapton membranes and a flow channel. Both Kapton membranes are 5 cm in diameter and vacuum metalized on one side with a 100 nm thick layer of aluminum. They form the flexible electrodes of two parallel plate capacitors. The two rigid electrodes are solid copper plates mounted $50\ \mu\text{m}$ away. The flow channel is a $4.8\ \mu\text{m} \times 0.27\ \mu\text{m}$ aperture in a $0.09\ \mu\text{m}$ thick silicon nitride membrane. The Si-Ni membrane is grown on the surface of a silicon wafer which is then etched to expose a $20\ \mu\text{m}$ square, freestanding Si-Ni window. The aperture is made in this window using electron beam

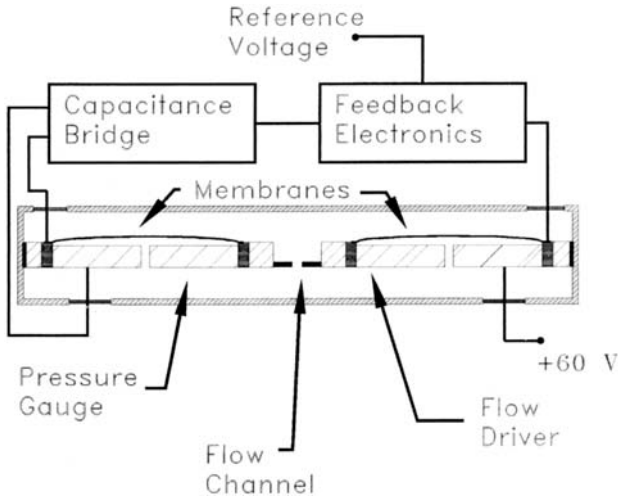


Fig. 1. Constant pressure-head flow cell.

lithography.⁷ The silicon chip is glued to a 50 μm thick copper foil which has been soldered to a copper ring. The assembly is mounted in the wall using indium seals.

The left capacitor is used as a calibrated pressure gauge which measures the pressure drop across the aperture. Because of the tension in the Kapton membranes, a pressure difference displaces them from their equilibrium positions. The displacement of the flexible electrode causes a shift in capacitance which is measured by a capacitance bridge. The output of the bridge is a voltage which is proportional to the pressure drop across the membrane, and thus the drop across the aperture. The pressure gauge is calibrated by applying a known electrostatic pressure and measuring the bridge output.

The right capacitor is used as a flow driver. The rigid plate is biased 60 V above ground and voltages in the range ± 12 V are applied to the flexible electrode. These voltages generate forces which displace the flexible electrode thereby generating the pressure drop across the aperture and driving flow through the aperture. The 60 V bias increases the displacement of the driver per volt applied to the flexible electrode and serves to somewhat linearize the displacement as a function of the voltage on the flexible electrode. The driver displacement is calibrated in the same manner as the pressure gauge.

The two flexible capacitors, capacitance bridge and feedback electronics form a system that can drive fluid through the aperture under constant pressure-head. When the feedback loop is locked, the feedback electronics apply voltage to the flexible electrode of the driver thereby displacing the pressure gauge. The feedback loop varies the voltage on the driver to keep the capacitance bridge output equal to the input reference voltage. After the transients have settled and the feedback circuit is holding the pressure gauge output constant, the pressure drop across the aperture is fixed and the driver is moving forward at a constant rate as it drives flow through the aperture. To displace the driver, the feedback voltage ramps up at a constant rate. Therefore, the derivative of the feedback voltage is a measurement of the supercurrent through the aperture. The system is able to drive up to $3.5 \times 10^{-9} \text{ m}^3$ of fluid at pressures as low as 0.5 mPa. The pressure resolution was limited by external vibrations. Each side of the cell is filled through a superleak tight cryovalve⁸ which is then closed to eliminate any free surfaces. The cell and valves are mounted on an internally cryopumped ^3He refrigerator capable of reaching 0.23 K. The temperature is measured with a nominal 100 Ω Matsushita carbon resistor which is calibrated *in situ* using ^3He vapor pressure thermometry. The resolution of the thermometer is approximately 1 mK. The thermometer was located outside of the cell and was not sensitive to the flow induced temperature difference.

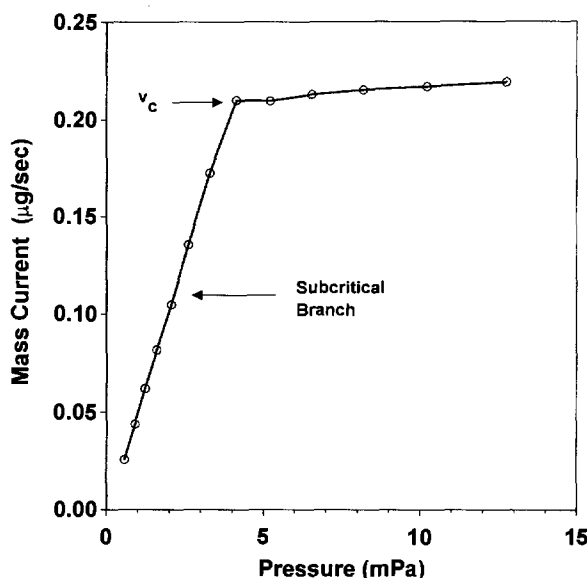


Fig. 2. Supercurrent versus applied pressure at 1.80 K. The line is only a guide for the eye.

In Ref. 1, it is shown that if the applied pressure difference is small and the channel at least partially locks the normal fluid, the superflow drives a temperature difference that eventually cancels the pressure contribution to the chemical potential. When the chemical potential difference becomes zero, the superfluid stops accelerating and v_s reaches a constant value that is below the critical velocity. This region corresponds to the subcritical resistive branch.⁹ This branch, as measured in our constant pressure-head flow cell, is shown in Fig. 2. The subcritical resistance, $\mathcal{R} \equiv \Delta P/i$, is a measure of the dissipation. It is determined by the inverse slope of a least squares fit of a line to the data on the subcritical branch. The resistance is plotted versus temperature in Fig. 3. The increasing scatter near T_λ is caused by a decreasing v_c and the finite resolution of the pressure gauge. To compare this data to the subcritical resistance given in Eq. 1, the only parameters needed are the normalized Kaptiza resistance¹⁰ and the surface areas of the two sides, 81 cm² and 240 cm². For the channel geometry used in this experiment, the viscous contribution to the resistance can be approximated by¹¹

$$R_\eta = \frac{4(\eta/\rho)}{\pi b a^2} \quad (3)$$

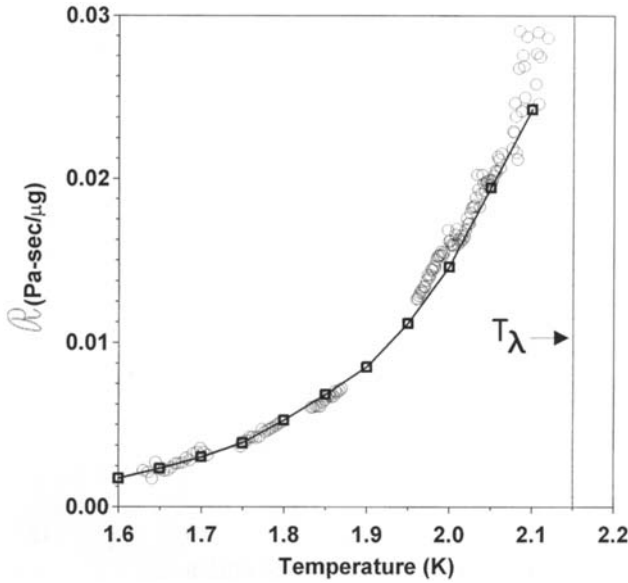


Fig. 3. Subcritical resistance. Circles: Measured resistance. Squares: Eq. 1. The resistance is evaluated every 0.05 K, the line is only a guide for the eye. The data is taken under a static pressure of approximately 2 atm.

where $a = 0.27 \mu\text{m}$ and $b = 4.8 \mu\text{m}$. For this channel, $R_\eta \gg \rho s^2 T R_T$ at all temperatures making the viscous contribution negligible. As was noted in Ref. 1, the expression for the viscous contribution is only valid when the mean free path of the excitations which make up the normal fluid is much smaller than the size of the aperture. Equation 1 is calculated every 0.05 K and is plotted over the experimental points in Fig. 3. The calculated curve contains no adjustable parameters. The specific entropy, density and viscosity are taken from other sources.¹²

4. OSCILLATING FLOW

Equation 2 gives the formula for the frequency response of a superfluid Helmholtz oscillator including the thermal effects of a superleak, normal fluid flow, compressibility, and thermal expansion. The derivation is quite lengthy, and we refer the reader to Ref. 1 for the details. The resonant frequency and Q of the oscillator can be extracted from this response. We have measured these quantities in three different Helmholtz oscillators^{5,6} over a wide range of temperature. Here, we will make a comparison

between the experimental data and the resonant frequency and Q extracted numerically from the frequency response. Also, we will derive useful analytical expressions for the resonant frequency and Q in experimentally important limits. The frequency response of one of the oscillators, which exhibits some interesting properties at frequencies below its resonance, is compared with the frequency response predicted in Ref. 1.

The three Helmholtz oscillators are generically the same. There are small differences in the methods of construction, but the essential differences are in the type of flow channel and the volume to surface area ratio of the baths which form the Helmholtz oscillator. The flow channels range from submicron apertures in silicon-nitride membranes to $100\ \mu\text{m}$ diameter tubes. The submicron apertures do not allow normal fluid flow and make thermal effects the most prominent. Since the major thermal resistance between the two helium baths is the Kapitza resistance, the volume to surface area ratio of the baths determine the time constants for the relaxation of the superflow-driven temperature difference. When the time constant is short, the temperature difference drives an irreversible heat flow into the walls. This causes dissipation which lowers the Q . When the time constant is long, the temperature difference can build up causing a significant fountain pressure. The fountain pressure opposes the motion of superfluid and leads to an upward shift in the resonant frequency. The larger diameter tubes allow normal fluid flow which leads to viscous damping of the oscillations, but a near cancellation of all thermal effects.

3.1. Single Aperture Oscillator (SAO)

As mentioned before the three Helmholtz oscillators are quite similar. Therefore, we will describe one of them in detail⁵ and only point out the important differences when discussing the other two. As shown in Fig. 4, the oscillator consists of a flexible; $8\ \mu\text{m}$ Kapton membrane which is glued over a $5\ \text{mm}$ square by $17\ \mu\text{m}$ deep recess that has been etched into the silicon cell body. The volume enclosed by the membrane and the recess forms the inner bath of the oscillator. This assembly is placed inside of a brass box which is sealed using indium. The volume between the outer box and the assembled oscillator forms the outer bath.

The silicon body has been etched in two steps. An initial etch forms the large recess that contributes the majority of the volume underneath the membrane. A second etch forms a pit which breaks through to the other side of the chip which has been previously coated with $100\ \text{nm}$ of silicon-nitride. This leaves a square, freestanding Si-Ni window which is approximately $30\ \mu\text{m}$ on a side. A small aperture, which serves as the flow channel, is made in this window using electron beam lithography.⁷ The

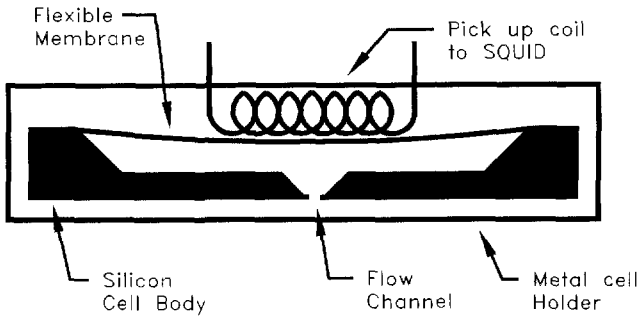


Fig. 4. Schematic diagram of the single aperture Helmholtz oscillator (SAO). The vertical dimension and membrane deflection are greatly exaggerated. The pickup coil is actually a spirally wound pancake coil which is glued to the metal cell holder. The gap between the pickup coil and membrane is roughly $50 \mu\text{m}$.

bottom of the large recess, which is vacuum metalized with 200 nm of gold, forms the rigid electrode of a parallel plate capacitor. The bottom side of the membrane is vacuum metalized with 100 nm of aluminum forming the flexible electrode. Voltages are applied to these electrodes to drive the oscillator. The top side of the membrane is sputtered with 200 nm of niobium forming the superconducting plane of a SQUID based detector¹³ which senses the motion of the membrane. The outer volume of the oscillator is filled through a superleak tight cryovalve⁸ which is then closed to isolate the cell acoustically and thermally. The inner volume fills through the flow channel. The cell and valve are mounted on an internally cryopumped ^3He refrigerator. The temperature is measured with a nominal 100Ω Matsushita carbon resistor which is calibrated against a commercially calibrated germanium resistor.¹⁴

Both the resonant frequency and Q of the Helmholtz resonance are measured as a function of temperature. At low temperatures where the Q is quite high, both parameters are obtained from a free decay of the oscillation. At high temperatures where the Q is lower, the resonant frequency (Q) is obtained from the peak (FWHM) of the frequency response of the oscillator. Data was not taken above 1.5 K because the low Q of the oscillator degraded its performance for the measurement it was originally designed.

For this oscillator, the flow channel consists of a $0.38 \mu\text{m} \times 1.25 \mu\text{m}$ aperture in a 100 nm thick Si-Ni window. The measured resonant frequency and Q are shown as the open triangles in Fig. 5. The thin line through the data is resonant frequency and Q extracted numerically from the calculated frequency response of Eq. 2. The resonant frequency is taken

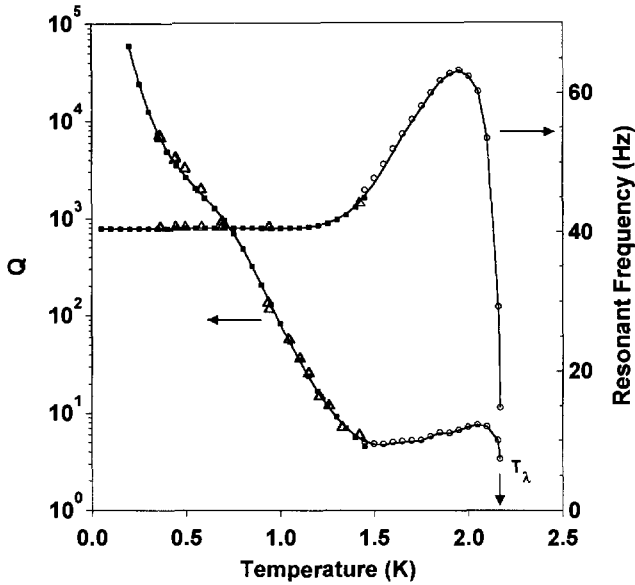


Fig. 5. Resonant frequency and Q for the Single Aperture Helmholtz Oscillator (SAO). Open triangles: Measured resonant frequency and Q . Solid squares: $\Gamma_h^2 \ll \Phi_h^2$ expansion given in Eq. 4. Open circles: $1 + \Gamma_h^2 \gg \Phi_h^2$ expansion given in Eq. 5. Solid line: Results extracted numerically from Eq. 2. Note: The theoretical expressions are only evaluated every 0.05 K. Data was not taken above 1.5 K.

to be the frequency at the maximum of the response and the Q is determined from the FWHM. With the exception of isothermal compressibility which is taken from Ref. 15, all of the thermodynamic data is taken from Ref. 12.

All of the cell parameters were fixed to the measured values except for the volume between the oscillator and the outer box. This volume was estimated to be 12 mm^3 . Varying this volume by a factor of 2 did not create a significant change in the calculated curves. Although the cell is not made from copper, the Kaptiza resistance is again taken from Ref. 10. To account for the difference in materials, a temperature independent scale factor is the only adjustable parameter used to fit the theoretical curve to the data. The theoretical curve in Fig. 5 was generated with a scale factor equal to 2.

The agreement between the numerical calculation and the experimental data is excellent, but it is useful to derive approximate analytical expressions for both the resonant frequency and Q . The aperture is quite small and the normal fluid is not expected to significantly contribute to the

total mass current. Mathematically, this can be seen from the function $G(R\sqrt{-i\omega\rho_n/\eta})$ which is defined in Eq. 27 of Ref. 1. The complex function G determines the degree to which the normal fluid is locked by its own viscosity. It ranges in magnitude from 0, where the normal fluid is locked and contributes no current, to 1, where the normal fluid is as important as the superfluid. Although G was derived assuming a circular tube, it can be used to give a rough estimate of the normal fluid contribution for this geometry. Using $R \approx 0.2 \mu\text{m}$ and $\omega \approx 240 \text{ rad/s}$, G takes on its maximum value of 3×10^{-4} near T_λ . Since G is quite small for all temperatures, the normal fluid can be safely ignored for this particular oscillator. The volume of this oscillator is small and the effects of compressibility are expected to be negligible. This is seen from the parameter Σ_{mc} which compares the spring constant of the membrane to the one due to the compression of the fluid. For this oscillator, $\Sigma_{mc} \approx 10^{-3}$. As discussed in Ref. 1, the small value of Σ_{mc} allows us to ignore the numerator of the frequency response when investigating the Helmholtz resonance. The parameters β and Σ_h take on a maximum absolute values of 5×10^{-3} near T_λ showing that the effects of thermal expansion are small. Ignoring these effects leaves only the thermal effects of superflow.

By neglecting these small effects, an approximate analytical expression for the resonant frequency can be obtained by finding the normalized frequency, Ω_{res} , at which the magnitude of the frequency response, $|1/H(\Omega_h, \dots)|$, is a maximum. The Q is then given by $\Omega_{res}^2/\text{Im}[H(\Omega_{res}, \dots)]$. We will consider two different limits, one that typically holds at low temperatures and another that holds at higher temperatures.

The parameter Γ_h^2 determines the size of the thermal effects. At low temperatures where the specific entropy is small, $\Gamma_h^2 \ll 1$. The thermal effects due to the superflow-driven temperature difference are expected to be small. The frequency response is expanded in terms of Γ_h^2 and the resonant frequency and Q of the oscillator are found to be

$$\begin{aligned}\omega_{res} &\approx \omega_{h0} \left[1 + \frac{\Gamma_h^2}{2(1 + \Phi_h^2)} \right] \\ Q &\approx \frac{1 + \Phi_h^2}{\Phi_h \Gamma_h^2} \left[1 + \frac{\Gamma_h^2}{2(1 + \Phi_h^2)} \right]\end{aligned}\tag{4}$$

For this oscillator, the expansion applies up to about 1.4 K. It is evaluated every 0.05 K and is plotted as the solid squares in Fig. 5.

At higher temperatures, the specific entropy is large, thermal effects dominate and the approximation $\Gamma_h^2 \ll 1$ no longer holds. Instead, we may use the approximation $1 + \Gamma_h^2 \gg \Phi_h^2$. The physical significance of this

approximation is explained below. The resonant frequency and Q are found to be

$$\begin{aligned} \omega_{res} &= \omega_{h0} \sqrt{1 + \Gamma_h^2} \left[1 - \frac{\Gamma_h^2}{4(1 + \Gamma_h^2)} \left(\frac{\Phi_h^2}{1 + \Gamma_h^2} \right) \right] \\ Q &= \frac{(1 + \Gamma_h^2)^{3/2}}{\Phi_h \Gamma_h^2} \left[1 - \frac{(\Gamma_h^2 - 2)}{4(1 + \Gamma_h^2)} \left(\frac{\Phi_h^2}{1 + \Gamma_h^2} \right) \right] \end{aligned} \tag{5}$$

Since $\omega_{res}^2 \approx \omega_{h0}^2(1 + \Gamma_h^2)$, this limit applies when $\omega_{res}^2 \gg 1/(R_T C_S)^2$. In other words, the oscillations are adiabatic. For this oscillator, the expansion applies from 1.4 K to T_λ . It is evaluated every 0.05 K and is plotted as the open circles in Fig. 5.

The previous results are consistent with Brooks *et al.*³ if an additional assumption is made. In Ref. 3, the oscillations were assumed to be adiabatic and the thermal effects were assumed to be small. In the language of this paper, this corresponds to $\Gamma_h^2 \ll 1$ and $\Phi_h \ll 1$. With this additional assumption, the leading order of Eqs. 5 is consistent with Eqs. 12 and 28 of Ref. 3. An additional term proportional to the thermal expansion appears in Ref. 3. It can be obtained from the present results by keeping the -2β term in the expansion of $1/H$.¹ Equation 31 of Ref. 3 gives an expression for the Q of the Helmholtz oscillator due solely to the viscous losses of the normal fluid which is assumed to be nearly completely locked. This result can be obtained from the present results if $1/H$ is expanded by keeping imaginary terms due only to G .¹ The assumption of a nearly locked normal fluid makes the argument of G small, and G can be expanded in terms of this argument.

These results may seem complicated, but they can be understood from a phasor representation of the forces on the membrane. In Ref. 1, Eq. 35 gives an expression for the amplitude of the effective force due to the superflow-driven temperature difference. Neglecting compressibility, it can be written as

$$\tilde{F}_{fountain} = -\Gamma_h^2 \frac{1 + i\Phi(\omega)}{1 + \Phi^2(\omega)} k\tilde{x} \tag{6}$$

This force is plotted on a phasor diagram in Fig. 6. It can be seen from Eq. 6 that Γ_h^2 is the parameter that determines the size of the thermal effects. As Γ_h^2 becomes larger, the thermal effects become more pronounced. But, Γ_h^2 does not reveal whether the thermal effects are reactive or dissipative. The normalized thermal time constant, $\Phi_h = \Phi(\omega_{h0}) = 1/(\omega_{h0} R_T C_S)$, provides this information. If $\Phi_h \gg 1$, heat is conducted through the Kapitza

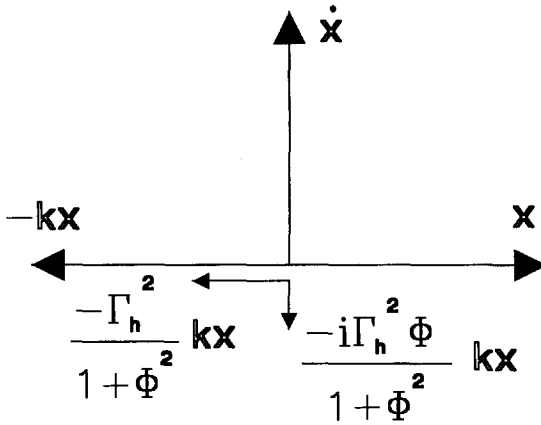


Fig. 6. Phasor diagram showing the relative amplitude and phase of the effective thermal forces.

resistance and the thermal effects are mostly dissipative. In Fig. 6, this corresponds to $\tilde{F}_{fountain}$ being mostly antiparallel to \dot{x} . When the thermal time constants are long, $\Phi_h \ll 1$, the superflow builds up a temperature difference with very little conduction through the cell wall. The temperature difference creates a fountain pressure which then acts back on the membrane effectively stiffening its spring constant. In Fig. 6, this corresponds to $\tilde{F}_{fountain}$ being mostly antiparallel to x . By examining the phasor diagram in the two previously mentioned limits, leading order of Eqs. 4 and 5 can be obtained.

3.2. Aperture Array Oscillator (AAO)

Although the construction of this oscillator differs slightly from the SAO, the main differences lie in the flow channel and the thermal relaxation time. The flow channel in this oscillator consists of 4225 square apertures, $0.1 \mu\text{m}$ on a side. They are laid out in a square array with a $3 \mu\text{m}$ center to center spacing. Since the apertures are reasonably close together, their flow fields interact. This interaction creates an effective length for each hole which is on the order of the size of the array and an effective area which is on the order of the square of the spacing between the apertures.¹⁶

As shown in Fig. 7, the body of this oscillator consists of an aluminum ring with an $8 \mu\text{m}$ Kapton membrane glued to one face. An annular Kapton spacer is glued over this membrane and another Kapton membrane is glued to the bottom of the spacer. The top membrane has a low spring

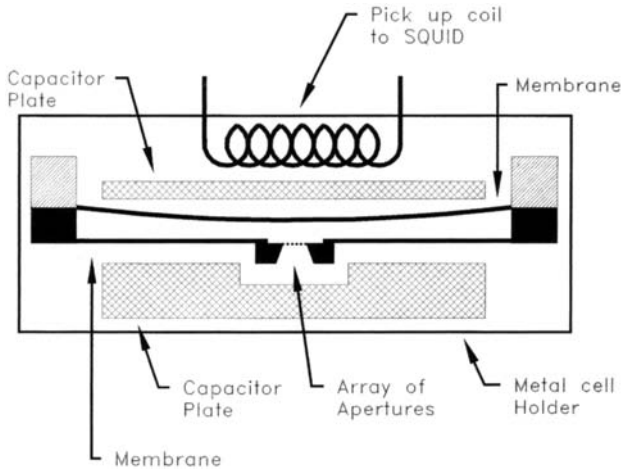


Fig. 7. Schematic diagram of the aperture array oscillator (AAO). The vertical dimension and membrane deflection are greatly exaggerated. The pickup coil is actually a spirally wound pancake coil which is placed roughly $150\ \mu\text{m}$ from the upper membrane. The spacing between the membranes is roughly $150\ \mu\text{m}$. The spacing between the membranes and their rigid capacitor plates is also $150\ \mu\text{m}$.

constant and its position is detected with a SQUID based position sensor¹³ similar to the one used in the SAO. A rigid electrode is mounted nearby to drive this membrane. The bottom membrane has a high spring constant. A small hole is cut in this membrane and a silicon chip containing the array of apertures is glued over the hole. A second rigid electrode is used to drive this membrane. The assembled oscillator is mounted inside of a metal cell holder. Although this cell has two membranes and therefore two resonant modes, the membranes are driven in such a way as to only excite the Helmholtz mode. This is accomplished by applying voltages to the two membranes so that the forces on the membranes are equal but oppositely directed. For this type of excitation, the ratio of the upper membrane displacement to the lower is k_l/k_u , and the two membranes behave as one with an effective spring constant of $k_l k_u / (k_l + k_u)$.

The cell is mounted on a cryostat which is dipped into a pumped helium bath. The Q and resonant frequency are measured from $1.3\ \text{K}$ to T_λ . The resonant frequency is taken to be the peak in the oscillator's frequency response and the Q is calculated from the FWHM. This data is shown as the open symbols in Fig. 8. The thin solid line shows the resonant frequency and Q extracted numerically from Eq. 2. The values are extracted every $0.05\ \text{K}$. The line is only a guide for the eye. There appear to be

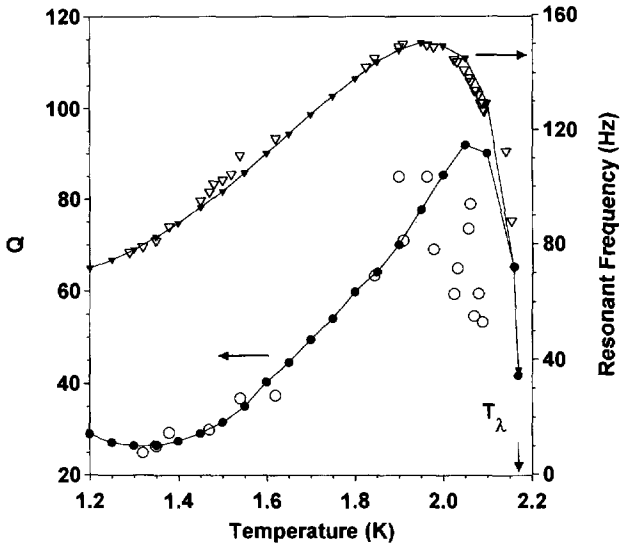


Fig. 8. Resonant frequency and Q for the Aperture Array Helmholtz Oscillator (AAO). Open circles: Measured Q . Open triangles: Measured resonant frequency. Solid symbols: $1 + \Gamma_h^2 \gg \Phi_h^2$ expansion given in Eq. 5. Solid line: Result extracted numerically from Eq. 2. Note: The theoretical expressions are only evaluated every 0.05 K.

systematic differences between the measured and calculated resonant frequency. This is most likely due to systematic errors in the measurement of the temperature. The Q data shows a large amount of scatter at the higher temperatures. This is result of the frequency response being recorded with rather coarse frequency resolution. Therefore, the linewidth could not be determined to high precision. Although the scatter in the data is large, the calculated Q agrees with the general trend of the data.

All of the cell parameters are fixed by the measured values except for the effective spring constant of the membranes and the inner volume of the oscillator. The effective spring constant is measured to be 1100 N/m. The spacing between the two membranes is set by Kapton spacer and cannot be measured after the cell is assembled. An estimate of the spacing yields an inner volume of 20 mm³. A better fit to the data is found with a spring constant of 1500 N/m and an inner volume of 50 mm³.

The AAO can be treated in a similar way to the SAO because estimates of the various terms in the frequency response reveal that G , Σ_{mc} , β and $\Sigma_h \ll 1$. Over the range of temperature where data was taken the approximation $1 + \Gamma_h^2 \gg \Phi_h^2$ holds. The expansion for this limit, Eq. 5, is plotted with filled symbols in Fig. 8.

A second difference between the SAO and the AAO lies in the volume to surface area ratio of the baths of helium. The gap between the two membranes in the AAO is approximately $300\ \mu\text{m}$. In the SAO, the gap between the membrane and the silicon chip is $17\ \mu\text{m}$. Since the transverse dimensions of these oscillators is much larger than the gap, the volume to surface area ratio is proportional to the gap. In this case, it can be shown that the thermal relaxation time is proportional to the gap. Therefore, the thermal time constant for the AAO is much larger and $\Phi_{\dot{h}}$ is smaller than for the SAO. At high temperatures where the thermal effects dominate, the effective thermal force has a much smaller dissipative component in the AAO. This accounts for the much higher Q in the AAO.

Because the thermal relaxation time is long, the AAO exhibits some interesting properties in its frequency response below the Helmholtz resonance. As seen from Fig. 6, when the frequency of the driving force is such that $\Phi(\omega) \approx 1$ the effective thermal force is 45° out of phase with $-k\tilde{x}$. At temperatures where thermal effects dominate, the result is a response which is up to 45° out phase with the drive. This force also acts to stiffen the membrane resulting in a decrease in the oscillator amplitude. In Fig. 9, the measured amplitude and phase response of the AAO is plotted. The calculated frequency response is plotted over the data as the solid lines. The agreement is quite good. The frequency response around compressional anti-resonance, ω_{c0} , is not presented because additional acoustic resonances ($\approx 500\text{--}700\ \text{Hz}$) within the cell holder complicated the identification of the various modes.

3.3. Large Diameter Tube Oscillator

The final oscillator⁶ has a construction nearly identical to the SAO, but the flow path consists of two channels instead of one. The major channel is made from a 4 mm long, $100\ \mu\text{m}$ inner diameter stainless steel tube that is glued into a hole etched through the silicon chip. An additional parallel channel consists of an approximately $0.1\ \mu\text{m} \times 0.7\ \mu\text{m}$ aperture in a Si-Ni window. The majority of the flow is through the stainless steel tube. Therefore, we will neglect the aperture in the rest of the discussion.

The resonant frequency and Q data are shown as the open symbols in Fig. 10. From the fact that there are oscillations above T_λ , the normal fluid must contribute significantly to the dynamics of the oscillator. This is confirmed by the function G^1 which has a magnitude as large as 0.8 near T_λ . The resonant frequency and Q extracted numerically from Eq. 2 are shown as the thin solid lines in Fig. 10. Except for a small discrepancy in the Q between 1.6 K and 2.0 K, the calculated curves agree with the data to within the experimental scatter.

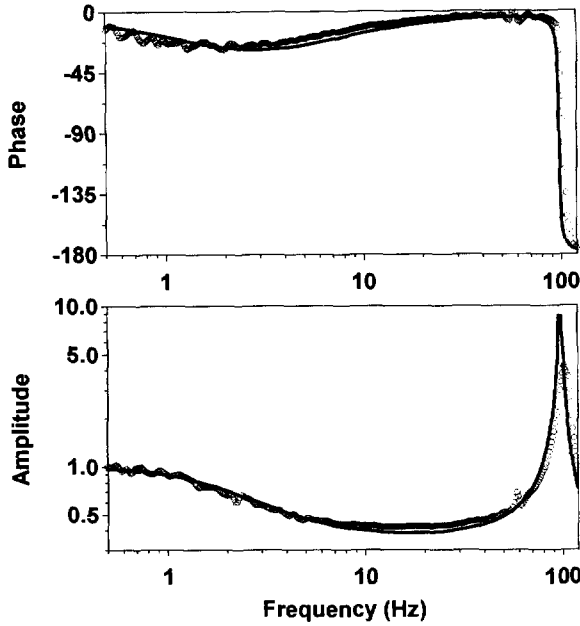


Fig. 9. Amplitude and phase response of the Aperture Array Oscillator (AAO) at 1.4 K. Open circles: Measured data. Thick line: Frequency response given by Eq. 2.

All of the cell parameters are fixed to the measured values except for the diameter of the stainless tube and the volume between the oscillator and the outer box. No attempt was made to measure the diameter which is specified by the manufacturer at $100\ \mu\text{m}$. The theoretical curves in Fig. 10 were generated with a diameter of $80\ \mu\text{m}$. The outer volume was estimated to be $50\ \text{mm}^3$. Varying this volume by a factor of 2 does not have a significant effect on the theoretical curves. The Kapitza resistance from Ref. 10 is multiplied by a temperature independent scale factor to account for the difference between copper and the materials used to construct the cell. The theoretical curves in Fig. 10 were generated with a scale factor of 1.75.

As discussed in Ref. 1, the normal fluid flow has multiple effects on the oscillator. If the normal fluid is completely locked and there are no thermal effects due to the superflow-driven temperature difference, the resonant frequency would vary with temperature as $\sqrt{\rho_s/\rho}$. The dash-dot curve in Fig. 10 shows this dependence. This behavior arises from the fact that the membrane displaces both normal and superfluid, but the hole only allows

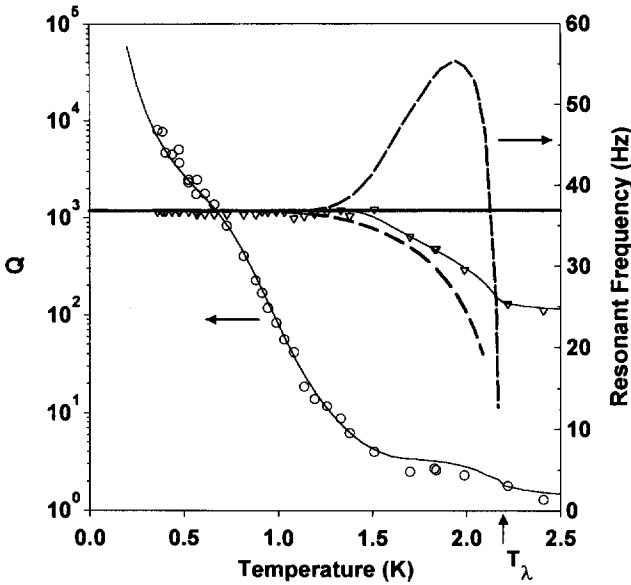


Fig. 10. Resonant frequency and Q for the large diameter tube Helmholtz oscillator. Open symbols: Measured Q and resonant frequency. Thin solid Lines: Results extracted numerically from Eq. 2. Dashed-Dot line: No normal fluid flow or thermal effects. Dashed line: No normal fluid flow. Thick solid line: Completely free normal fluid. Note: The theoretical expressions are only evaluated every 0.05 K.

superflow. If the normal fluid was completely free, this temperature dependence would be completely cancelled and the resonant frequency would be given by the thick solid line in Fig. 10. For this particular oscillator, $Re(G) \approx 0.7$ near T_λ giving a resonant frequency which falls somewhat below the thick solid line. A second effect of normal fluid flow is the cancellation of the superflow-driven temperature difference. If the normal fluid is completely locked but we include thermal effects due to the superflow, the resonant frequency would display the characteristic upturn as shown by the dashed curve in Fig. 10. If the normal fluid were completely free, the two mass currents would flow as to not change the ratio of super to normal component in the two baths. There would be no temperature difference and no thermal effects. Since this oscillator does allow a large amount of normal fluid flow, there is no large increase in the resonant frequency at the higher temperatures. Finally, the normal fluid dissipates energy due to its viscosity. Near T_λ , the $Re(G) \approx 0.7$, but the $Im(G) \approx 0.2$. In this case, the normal fluid is still quite damped as seen by

the low Q around T_λ . At lower temperatures, the viscous penetration depth for the normal fluid grows. This locks the normal fluid in tubes even as large as $100\ \mu\text{m}$. This is why the Q at lower temperatures resembles the data for the SAO.

4. CONCLUSIONS

Various mechanisms have been considered which affect the flow of superfluid ^4He through constrictions. For small volume Helmholtz oscillators with small aperture flow channels, the superflow-driven temperature difference was found to significantly increase the resonant frequency. The temperature difference also causes dissipation by driving a heat current through the walls of the cell. This mechanism is also responsible for the subcritical dissipation observed in constant pressure-head flow cells. For oscillators with flow channels made from larger diameter openings, the partial motion of the normal fluid raises the resonant frequency above ω_{h0} and also partially cancels the increase in frequency due to thermal effects.

The results in this paper, both numerical and approximate expansions, agree very well with the measured subcritical resistance of a constant pressure-head flow cell and with the Q and resonant frequency of Helmholtz oscillators. This quantitative agreement between the calculations and experimental data provides an excellent check of their equations derived to describe this type of flow.

ACKNOWLEDGMENTS

One of the authors (S.B.) would like to thank Ekaterina Backhaus for assistance with parts of the computer code used in this work. This work was sponsored by the Office of Naval Research, NSF, and NASA. The experimental work on the AAO was sponsored in part by ONR contract number N00014-94-1008.

APPENDIX

Here, we define symbols used in this paper. The notation is the same as Ref. 1.

T = temperature

s = entropy per unit mass

ρ = total fluid mass density

ρ_s = superfluid mass density

- ρ_n = normal fluid mass density
 η = normal fluid viscosity
 κ = isothermal compressibility
 α = thermal expansion coefficient
 c_p = heat capacity per unit mass at constant pressure
 k = membrane spring constant
 A = area of the membrane
 a = cross sectional area of the flow channel
 R = radius of the flow channel
 l_{eff} = total hydraulic length of the flow channel
 M_i = mass of helium in bath i
 $C_S = (1/C_1 + 1/C_2)^{-1}$ where C_i is the total heat capacity of helium bath i
 R_T = total Kapitza resistance from helium bath 1 to bath 2
 $\Sigma_{mc} = (k\kappa M_1 M_2) / [\rho A^2 (M_1 + M_2)]$
 ω = angular frequency of oscillation
 $\omega_{h0} = \sqrt{\rho_s a k / [\rho^2 l_{\text{eff}} A^2 (1 + \Sigma_{mc})]}$
 Q = quality factor of Helmholtz oscillator
 $\Phi(\omega) = 1 / (\omega R_T C_S)$
 $\Phi_h = 1 / (\omega_{h0} R_T C_S)$
 $\Gamma_h^2 = \rho^2 s^2 T A^2 (1 + \Sigma_{mc}) / (k C_S)$
 $\beta = \alpha s T / c_p$
 $\Sigma_h = [\alpha^2 T / (\rho \kappa c_p)] [\Sigma_{mc} / (1 + \Sigma_{mc})]$
 i = total mass current
 ΔP = pressure drop across flow channel
 R_n = ratio of pressure to mass current for steady flow of a viscous fluid of density ρ through a channel

REFERENCES

1. S. Backhaus and E. Yu. Backhaus, *J. Low Temp. Phys.* **109**, 511 (1997).
2. J. Wilks, *The Properties of Liquid and Solid Helium*, Clarendon Press, Oxford (1967), Section 13.8.
3. J. S. Brooks, B. B. Sabo, P. C. Schubert, and W. Zimmermann, Jr., *Phys. Rev. B* **9**, 4524 (1979).
4. S. Backhaus and R. E. Packard, Proceedings of LT-21, *Czech. J. of Phys.* **46(S5)**, 2743 (1996).
5. J. Steinhauer, K. Schwab, Y. Mukharsky, J. C. Davis, and R. E. Packard, *J. Low Temp. Phys.* **100**, 281 (1995).
6. K. Schwab, J. Steinhauer, J. C. Davis, and R. E. Packard, *J. of Microelec. Syst.* **5**, 180 (1996). The oscillator in this reference has a slightly different flow channel than the one used to take the data for this paper.
7. A. Amar, Y. Sasaki, R. Lozes, J. C. Davis, and R. E. Packard, *J. Vac. Sci. Tech. B* **11**, 259 (1993).
8. N. Bruckner, S. Backhaus, and R. E. Packard, Proceedings of LT-21, *Czech. J. of Phys.* **46(S5)**, 2741 (1996).

9. G. M. Shifflett and G. B. Hess, *J. Low Temp. Phys.* **98** (5/6), 591 (1995); S. Backhaus, N. Bruckner, A. Loshak, K. Schwab, and R. E. Packard, Proceedings of LT-21, *Czech. J. of Phys.* **46(S1)**, 127 (1996).
10. L. J. Challis, K. Dransfeld, and J. Wilks, *Proc. Roy Soc. Lond.* **A260**, 31 (1961).
11. P. M. Morse and H. Feschbach, *Methods of Theoretical Physics*, McGraw-Hill, New York (1953), p. 1197.
12. R. J. Donnelly, R. A. Riegelmann, and C. F. Barenghi, *The Observed Properties of Liquid Helium at the Saturated Vapor Pressure*, A Report to the Department of Physics, University of Oregon. Eugene, Oregon, 1992.
13. H. J. Paik, *J. Appl. Phys.* **47**, 1168 (1976).
14. Lake Shore Cryotronics, Inc. Model #: GR200A-50.
15. J. S. Brooks and R. J. Donnelly, *J. Phys. and Chem. Ref. Data* **6**, 51 (1977).
16. J. S. Brooks, B. B. Sabo, P. C. Schubert, and W. Zimmermann, Jr., *Phys. Rev. B* **19**, 4524 (1979).